Accurate determination of respiratory rhythm and pulse rate using an under-pillow sensor based on wavelet transformation

Accurate Determination of Respiratory Rhythm and Pulse Rate Using an Under-Pillow Sensor Based on Wavelet Transformation

Xin Zhu[1], Wenxi Chen[1], Tetsu Nemoto[2], Yumi Kanemitsu[3], Kei-ichiro Kitamura[2], and Ken-ichi Yamakoshi[4]
1.Graduate Department of Information Systems, the University of Aizu, Aizu-wakamatsu, Fukushima, Japan; 2.Graduate School of Medical Science, Kanazawa University, Kanazawa, Ishikawa, Japan; 3.SRI Research & Development Ltd., Kobe, Hyogo, Japan; 4.Faculty of Engineering, Kanazawa University, Kanazawa, Ishikawa,

***Abstract*—A real-time noninvasive and unconstrained method is proposed to determine the respiratory rhythm and pulse rate with an under-pillow sensor during sleep. The sensor is composed of two fluid-filled polyvinyl tubes set in parallel and sandwiched between two acrylic plates. One end of each tube is hermetically sealed, and the other end is connected to one of two pressure sensors. Inner pressure in each tube therefore changes in accordance with respiratory motion and cardiac beating. By employing the *á trous* algorithm of wavelet transformation (WT), the respiratory and cardiac cycle can be discriminated from the pressure waveforms. The respiratory rhythm was obtained from the WT 2^6 scale approximation, and the pulse rate from the sum of WT 2^4 and 2^5 scale details without WT reconstruction after soft-threshold denoising. The algorithm's latency can be set to be minimal and the respiratory rhythm and pulse rate were estimated directly from the extracted respiration and pulse waveforms, respectively. This method has been tested with a total of about 25 h data collected from 13 subjects. By comparing the detection results with those of reference data, the average pulse rate detection sensitivity and positive predictivity were 99.11% and 98.51%, and the respiratory rhythm detection sensitivity and positive predictivity were 95.40% and 95.07%.**

***Index Terms*—Pulse rate, respiration rhythm, sleep monitoring, unconstrained monitor, wavelet transformation**

I. Introduction

The real-time monitoring of both respiratory rhythm and heart rate during sleep plays an important role in the diagnosis and treatment of sleep apnea and sudden death syndrome. There are numerous traditional methods for respiratory measurement, including spirometry, nasal temperature sensing, body plethysmography, impedance pneumography, strain-gauge or inductance-type plethysmography, and ECG-based derived respiration methods [1]. These methods, however, may bring discomfort and inconvenience to the subject as well as to the physician, owing to procedures necessary for attaching sensors to the body. Conventional heart rate monitoring using ECG, heart sound, and finger photoelectric plethysmogram (FPP), also require appropriate sensors to be attached to subjects.

In contrast to these methods, a pillow-based respiratory rhythm or pulse rate monitoring method has recently been developed without direct attachment of any sensors to the body [2-4]. In our previous system [4], the respiratory rhythm and pulse rate from pressure signals acquired from two fluid-filled tubes under the pillow were obtained by filtering the raw signals which contained respiratory components (about 10–20/min) and pulse rate (about 50–80/min). However, a low-pass filter with such a low and narrow band-pass is not easy to design and of a high order. The respiratory and cardiac pulse components, as well as motion artifacts and noises superimposed on the raw pressure signals, will greatly hinder the accurate estimation of the respiration rhythm and pulse rate. Uchida et al. [5] have applied the independent component analysis (ICA) to separate noise from the two signals. However, because of the phase difference of the respiratory and pulse waveforms in the two signals, the source instantaneous mixture hypothesis of ICA is not satisfied. Therefore, the respiratory and pulse waveforms cannot be sufficiently separated using the ICA method. In addition, the power spectrum density analysis is also difficult to provide beat-by-beat estimations and can be easily influenced by noise and artifacts [6].

On the other hand, wavelet transformation (WT) has been widely applied in the biomedical signal-processing field [7-9]. In particular, WT multi-resolution analysis has been found to be effective in removing non-white or high-frequency noise [10], detecting ECG characteristic points [11], performing data compression [12], extracting the fetal ECG [13], and delineating ECG [14].

This paper describes a real-time method based on the WT *á trous* algorithm [15] to accurately obtain the respiratory rhythm and pulse rate from the pressure signal acquired using a fluid-filled tube under a pillow. The raw signal is decomposed into different scale components with the WT *á trous* algorithm by neglecting the down-sampling procedure. After suppressing noise with a soft-threshold de-noising method, respiratory and pulse waveforms can be obtained from the approximation and detail components without reconstruction from their respective characteristic scales. By employing the characteristic point detection method, the respiratory rhythm and pulse rate can be obtained from the extracted respiratory and pulse waveforms.

II. Methodology

A. Measurement System and Signal

A schematic of the measurement system is shown in Figure 1. Two incompressible polyvinyl tubes, 30 cm in length and 2 cm in diameter, are filled with air-free water preloaded with an internal pressure of 3 kPa and have a 15 cm-long arterial catheter connected in one end. The two fluid-filled polyvinyl tubes are set in parallel 13 cm away from each other and sandwiched between two acrylic plates. One end of each tube is hermetically sealed and the other end is connected to one of two pressure sensors (KEYENCE Corp., AP-13). Inner pressure in each tube changes in accordance with respiratory motion and

cardiac beating. Filtered pressure signals (0.16-5.0 Hz) are digitized into a PC through a 16-bit analogue-to-digital (A/D) converter board and stored. The pillow is stuffed with numerous fragments of soft material made of synthetic resins. Signals can be collected while sleeping in a supine or recumbent position. FPP and nasal thermistor measurements are recorded as reference data. The sampling rate is 100 Hz for all four signals.

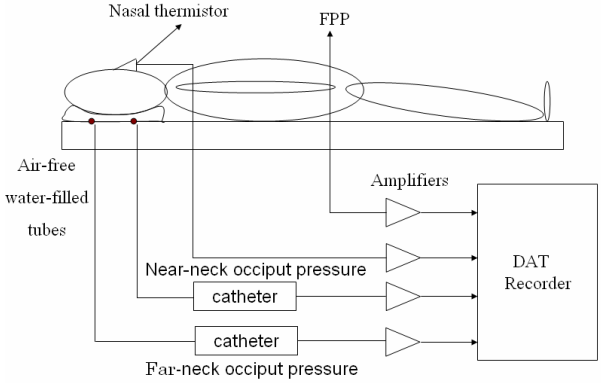

Fig. 1 The under-pillow fluid-filled tube sensor and measurement system.

B. *Subjects and signals*

The near- and far-neck occiput pressures, and reference data were collected from 13 subjects (five female and eight male college students, 21-22 years' old) at the School of Health Sciences, Kanazawa University, Japan. Approximately 2 h of data were acquired from each subject during sleep. Figure 2 shows 40.96 s of representative measured signals. The upper two rows display pressure signals in the far-neck occiput (Fig. 2a) and near-neck occiput (Fig. 2b). The lower two rows are FPP (Fig. 2c) and nasal thermistor (Fig. 2d) signals.

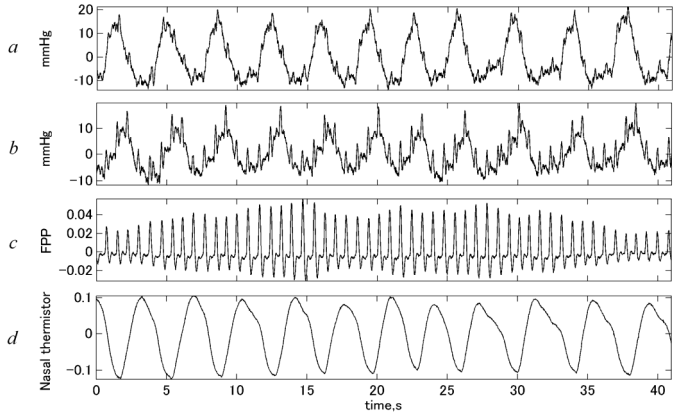

Fig. 2 Four directly measured signals: (a) far-neck occiput pressure, (b) near-neck occiput pressure, (c) finger photoelectric plethysmogram (FPP) and (d) nasal thermistor signals. (a), (b) are pressure signals, and (c), (d) serve as reference data. Each is 40.96 s in time.

C. *Principle of wavelet transformation*

The wavelet transformation (WT) of $x_2(t)$ is as follows,

$$W_s x_2(t) = \frac{1}{s}\int_{-\infty}^{+\infty} x_2(\tau)\psi(\frac{t-\tau}{s})d\tau \qquad (1)$$

where s is the scale factor and $\psi(t)$ is the prototype wavelet function. It is called a dyadic WT if $s = 2^j$ (j=Z, Z is the integral set) [8]. Two filters, the low- and high-pass decomposition filters, $\mathbf{H}_0(z)$ and $\mathbf{H}_1(z)$, and associated reconstruction filters, $\mathbf{G}_0(z)$ and $\mathbf{G}_1(z)$, can be derived from the prototype wavelet and its scale function with the Mallat algorithm. In this paper, the *á trous* algorithm is employed to extract the respiratory and pulse waveforms from the pressure signal. Unlike the Mallat algorithm, the *á trous* algorithm is time-invariant and has the same temporal resolution in every scale [16]. The *á trous* algorithm neglects the down-sampling and up-sampling procedures and the low- and high-pass filters in the $s = 2^j$ scale are replaced by $\mathbf{H}_0(z^s)$, $\mathbf{H}_1(z^s)$, $\mathbf{G}_0(z^s)$, and $\mathbf{G}_1(z^s)$ [15]. The *á trous* algorithm decomposition low- and high-pass filter coefficients, $\mathbf{h}_{0,j+1}$ and $\mathbf{h}_{1,j+1}$, are the inverse $\mathbf{Z}$ transformation of $\mathbf{H}_0(z^s)$ and $\mathbf{H}_1(z^s)$, respectively.

The decomposition procedure is as follows,

j=0;
while j<**J**
  $\mathbf{d}_{j+1}=\mathbf{a}_j * \mathbf{h}_{1,j+1}$;
  $\mathbf{a}_{j+1}=\mathbf{a}_j * \mathbf{h}_{0,j+1}$;
  j=j+1;
end

Where **J** is the number of the largest scale layer, $\mathbf{a}_j$ is the 2^j scale approximation, $\mathbf{d}_j$ is the 2^j scale detail, and $\mathbf{a}_0$ is the raw signal. In this paper, the CDF (9,7) biorthogonal wavelet is selected as the prototype wavelet to design the decomposition and reconstruction filters [17]. The CDF (9,7) biorthogonal wavelet has compact support, four vanishing moments, and is promoted by JPEG2000 [18]. The filters are symmetrical and have a linear phase shift. Therefore, the time delay can be estimated easily and adjusted for real-time processing.

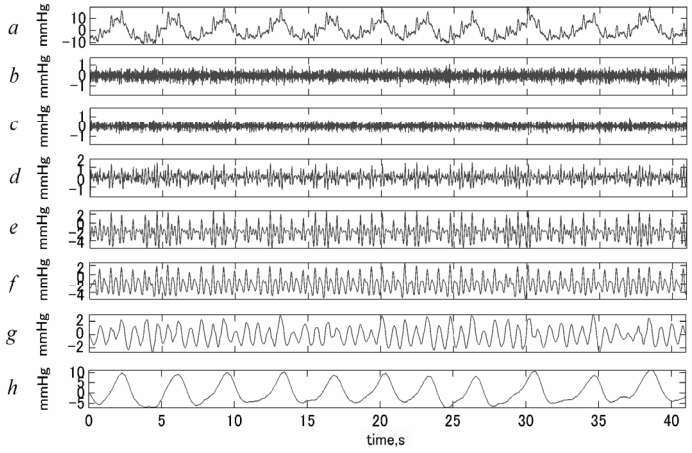

Fig. 3 Wavelet decompositions of pressure signal from the sensor in near-neck occiput region. (a) Raw signal (near-neck occiput pressure). (b)-(g) Waveforms from detail components in 2^j (j=1-6) scales, respectively. (h) Waveforms from approximation components in 2^6 scale.

Figure 3 shows the decomposed components of the pressure signal measured under the near-neck occiput. The time delay of each filter is removed from the decomposed components in every scale. The raw signal shown in Figure 3a (the same as in Fig. 2b) is decomposed into s=2^j, (j=1-6) scales. It is observed that the 2^6 scale approximation (Fig. 3h) is close to the nasal thermistor signal (Fig. 2d), and the 2^4 and 2^5 scale detail components (Fig. 3e and 3f) contain peaks similar to those of the pulse waveform in the FPP. This indicates that the 2^6 scale

approximation (about 0 to 0.8 Hz) can be used to obtain the respiratory rhythm (about 0-1 Hz), and the pulse rate can be synthesized from the 2^4 and 2^5 scale details (about 1.6 to 6.2 Hz). Conventionally, the respiratory and pulse waveforms should be reconstructed from the 2^6 scale approximation, and 2^4 and 2^5 scale details, respectively. However, by using the *á trous* algorithm, we found that it is possible to obtain the respiratory and pulse waveforms without the reconstruction. That is, the 2^6 scale approximation can be used to represent the respiratory waveform, while the sum of the 2^4 and 2^5 scale details can be used to represent the pulse waveform after the noise is removed using soft-threshold denoising [8-9]. In this paper, the denoising threshold is $0.2\sigma_4$ for the 2^4 scale detail, and $0.1\sigma_5$ for the 2^5 scale detail. σ_j is the standard deviation of the 2^j scale detail. The real-time algorithm is realized by processing a specific duration signal segment sequentially with the wavelet transformation. The processed signal segments are then catenated with the overlap-add method to estimate the respiratory rhythm and pulse rate. The duration of the signal segment can be determined to be any feasible value in view of the real-time requirement. The algorithm for detecting the pulse rate from the FPP and extracted pulse waveform is a refinement of the ECG peak detection methods [19]. To detect characteristic points from the FPP and extracted pulse waveform, signals are filtered through a first-derivative operator, and then points corresponding to the pulse peaks are determined by an algorithm with a locally adaptive threshold and search back protocol. The characteristic points in the nasal thermistor signal and extracted respiratory waveform are defined as the upward zero-cross point. The zero line is locally adapted to track the baseline drift, and the upward zero-cross points with sufficiently deep preceding valleys are recognized as characteristic points in the respiratory waveform. Figure 4a is the raw pressure signal in the near-neck occiput. Figures 4b–4e show the FPP signal, extracted pulse waveform, nasal thermistor, and extracted respiratory waveform (their detected characteristic points are marked with "•" in the figure). Before detection of the characteristic points, artifacts caused by body movements are detected using an adaptive threshold method. When an extremely large value, compared with the highest value and standard deviation of the preceding raw signal, is found in the raw pressure signal, the preceding and proceding 3 s raw pressure signals are neglected and not used for the analysis.

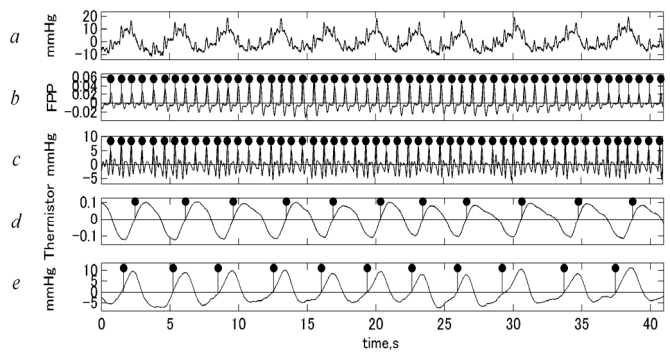

Fig. 4 Extracted signals corresponding to pulse and respiration rhythms, and detected characteristic points. (a) Raw signal, (b) FPP, (c) Extracted pulse waveform, (d) Nasal thermistor signal, (e) Extracted respiration waveform.

III. Evaluation and Results

The detection evaluation method is described as follows,

The number of peaks in the pulse and upward zero-cross points in the respiratory signal are counted sequentially for every minute. The total false positive number (*TFP*) increases with the number of extra characteristic points when the detected characteristic point number in the reference signal is less than that in the derived signal in a minute; the total false negative number (*TFN*) increases with the number of missing characteristic points when the detected characteristic point number in the reference signal is more than that in the derived signal in a minute. The total characteristic point number in the reference signal is *TPR*, and the total characteristic point number in the extracted signal is *TPE*. The total real positive characteristic point number *(TRP)* equals *TPE-TFP*. The average *FN rate* is *TFN*/*TPR*, and the average *FP rate* is *TFP*/*TPR*. The positive predictivity P^+ is defined as *TRP*/(*TRP*+*TFP*), and the sensitivity *Se* is *TRP*/(*TRP*+*TFN*).

Figure 5 shows a subject's profile of the respiratory rhythm and pulse rate estimation results and relative errors. Tables 1 and 2 show the statistics of the estimation results.

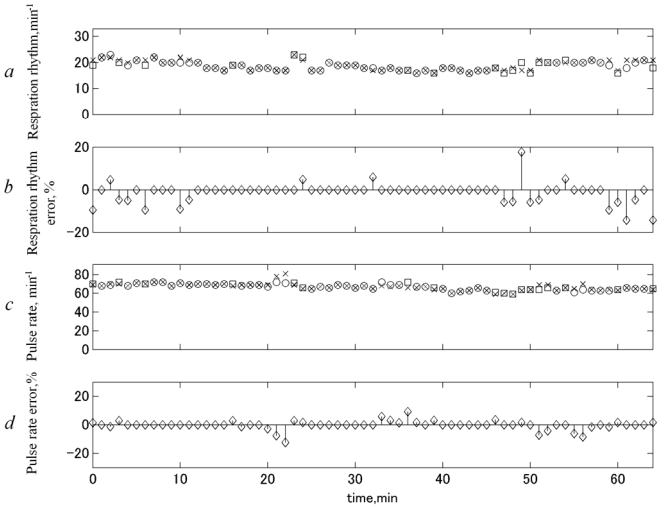

Fig.5 Instantaneous profiles of (a) respiration rhythm and (c) pulse rate detected from the extracted waveforms (○ or □) and the reference data (×); and estimation errors of (b) respiration rhythm and (d) pulse rate. ○ indicates the value is detected when there is no artifact at that minute. □indicates there are artifacts at that minute and the value shown is the average respiration rhythm or pulse rate estimated from the artifact-free signal at that minute.

Table 1. Pulse beat detection results from FPP and extracted pulse waveforms

Subject	Time (min)	Pulse beat detected		False rate (%)	
		FPP	Extracted	Negative	Positive
1	131.7	7409	7508	1.82	3.16
2	133.4	9268	9248	0.58	0.37
3	66.7	4719	4739	0.21	0.64
4	48.3	2813	2862	0.04	1.78
5	66.7	3681	3701	0.16	0.71
6	133.4	6843	6855	0.06	0.77
7	100.0	4901	4958	1.98	3.14
8	266.0	17484	17726	0.50	1.88
9	133.4	9046	9080	0.93	1.31
10	128.7	6031	6129	0.36	1.99
11	66.7	5158	4937	4.81	0.52
12	33.3	1934	1970	0	1.86
13	186.7	11529	11663	0.16	1.33
Total	1495.0	90816	91376	0.89	1.50

Se = 99.11%, P^+=98.51%

Table 2. Respiratory rhythm detection results from nasal thermistor and extracted respiration waveforms

Subject	Time(min)	Respiration detected		False rate (%)	
		Thermistor	Extracted	Negative	Positive
1	131.7	1601	1786	5.44	16.99
2	133.4	2456	2395	2.77	0.29
3	66.7	1014	911	11.34	1.18
4	48.3	919	781	15.56	0.54
5	66.7	906	923	1.21	3.09
6	133.4	1921	1913	3.49	3.07
7	100.0	1382	1349	3.33	0.94
8	266.0	3853	3874	3.01	3.55
9	133.4	2157	2151	6.72	6.44
10	128.7	2244	2374	1.20	7.00
11	66.7	770	748	5.32	2.47
12	33.3	604	567	10.93	4.80
13	186.7	3202	3337	4.00	8.21
Total	1495.0	23029	23109	4.60	4.95

Se = 95.40%, P^+=95.07%

IV. DISCUSSION

From Tables 1 and 2, it can be seen that the *FN rate* is lower than the *FP rate* in the respiratory rhythm and pulse rate estimation. This shows that the proposed method will detect a relatively higher respiratory rhythm and pulse rate than the real values. The detection errors in the respiratory rhythm are higher than in the pulse rate, which is more likely to be more accurately estimated.

The detection error mainly comes from:

(1) Movement artifacts.

The measurement of pressure signals is not as stable or reliable as the FPP or nasal thermistor signals. Extra characteristic points will be incorrectly detected when there are artifacts, such as head and body movements, which are the main reason that the *FN rate* is lower than the *FP rate*.

(2) Sensor loss

When the sensor is not well installed under the head, the pressure signal cannot be measured. At such times, the algorithm cannot detect characteristic points. This will increase the *FN rate*.

(3) Characteristic point

It was found that the low-frequency respiratory waveform is more likely to be influenced by the low-frequency body movement artifacts. Furthermore, as the peak in the pulse rhythm is more likely to be accurately detected than the upward zero-cross point in the respiratory rhythm, the accuracy and reliability of the pulse detection is naturally better than those of the respiratory.

To decrease the detection error, the sensor and algorithm should be further modified and improved to provide a more reliable and accurate estimation of the respiratory rhythm and pulse rate.

V. CONCLUSION

This paper proposes a noninvasive and unconstrained method to measure the respiratory rhythm and pulse rate from only one pressure signal, measured during sleep. The pressure signal is decomposed into its detail and approximation components using the WT *á trous* algorithm. The respiratory rhythm can be obtained from the high scale approximation component, while the pulse rate can be attained from the detail components after the noise is removed using a soft-threshold denoising method. The characteristic points in the extracted respiratory and pulse waveforms can be detected to estimate the respiratory rhythm and pulse rate. For the measurement of the pulse rate, *Se* 99.11% and P^+ 98.51% can be achieved. For the measurement of respiratory rhythms, *Se* 95.40% and P^+ 95.07% can be obtained. It has been proven that the respiratory rhythm and pulse rate can be estimated accurately and reliably. This may become a reliable and simple method to monitor the sleep apnoea and sudden death syndrome during sleep. Furthermore, combining EEG analysis with this method will provide a powerful and convenient approach to study the relationship between EEG activity, sleep stage, respiration rate, and pulse rate.

ACKNOWLEDGMENT

The authors are grateful to those students at the School of Health Sciences, Kanazawa University, for their efforts in data collection.

REFERENCES

[1] G.B. Moody, R.G. Mark, A. Zoccola, and S. Mantero, "Derivation of respiratory signals from multi-lead ECGs", *IEEE Comp. Card.*, vol. 12, pp. 113–116, 1985.

[2] K. Nakajima, H. Yamakose, H. Kuno, M. Nambu, T. Irie, M. Higuchi, A. Sahashi, and T. Tamura, "A pillow-shaped respiration monitor", *Life Suppo.*, vol. 13, pp. 2-7., 2001

[3] K. Nakajima, H. Yamakose, H. Kuno, M. Nambu, T. Irie, M. Higuchi, A. Sahashi, and T. Tamura, "Evaluation for sleep apnea syndrome by a pillow-shaped respiration monitor", *Life Suppo.*, vol. 14, pp. 14-19, 2002

[4] K. Watanabe, T. Tasaki, T. Nemoto, YAMAKOSHI, K. Yamakoshi, and W. Chen, "Development of biometry system in the sleep by pillow cuff installed on the occiput", *Japan Soc. ME&BE Trans.*, vol. 41, Suppl. 1, pp. 168, 2003

[5] M. Uchida, S. Ding, W. Chen, T. Nemoto, and D. Wei, "An approach for extractions of pulse and respiration information from pulsatile pressure signals", *Proc. IEEE Asia-Pacific BME conf.*, Kyoto, CDROM, 2003

[6] Y. Kanemitsu, Y. Yamashita, T. Nemoto, S. Takada, K. Kitamura, K. Yamakoshi, and W. Chen, "Development of biometry system in the sleep", *Proc. of the 43rd annual conf. of Japanese Society for ME & Biol. Eng.*, Kanazawa, Japan, CDROM, 2004

[7] S. Mallat, and W.L. Hwang, "Singularity detection and processing with wavelets", *IEEE Trans. IT*, vol. 38, pp. 617-643, 1992

[8] S. Mallat, and S. Zhong "Characterization of signals from multi-scale edges", *IEEE Trans. PAMI*, vol. 14, pp. 710-732, 1992

[9] M. Akay, "Time frequency and wavelets in biomedical signal processing", IEEE Press, New York, 1998

[10] C. Taswell "The what, how, and why of wavelet shrinkage denoising", *IEEE Magazine*, *Comp. Sci. Eng.*, pp. 12-19, May/June 2000

[11] C. Li, C. Zheng, and C. Tai: 'Detection of ECG characteristic points using wavelet transformation', *IEEE Trans. BME*, vol. 42, pp. 21-28, 1995

[12] M.L. Hilton, "Wavelet and wavelet packet compression of electrocardiograms", *IEEE Trans. BME*, vol. 44, pp. 394-402, 1997

[13] A. Khamene, and S. Negahdaripour, "A new method for the extraction of fetal ECG from the composite abdominal signals", *IEEE Trans. BME*, vol. 47, pp. 507-516, 2000

[14] J. P. Martinez, Almeida, R., Olmos, S., Rocha A.P., and Laguna P. "A wavelet-based ECG delineator: evaluation on standard databases", *IEEE Trans. BME* 40**:** 2464-2484, 2004

[15] M.J. Shensa, "The discrete wavelet transformation-wedding the á trous and the Mallat algorithm", *IEEE Trans. SP*, vol. 40, pp. 2464-2484, 1992

[16] A.P. Bradley, "Shift-invariance in the discrete wavelet transforms", *Proc.7th Digital Imaging Computing: Tech. and Appli.*, Sun C., Talbot H., Ourselin S. and Adriaansen T. (Eds.), Sydney, pp. 10-12, Dec. 2003

[17] I. Daubechies, Ten lecture on wavelets. SIAM: Philadelphia, PA, 1992

[18] M. Unser, and T. Blu, "Mathematical property of the JPEG2000 wavelet filters", *IEEE Trans. IP*, vol. 12, pp. 1080-1090, Sep. 2003

[19] J. Pan, and W.J. Tompkins, "A real-time QRS detection algorithm", *IEEE Trans. BME*, vol. 32, pp. 230-236, 1985